Third International Symposium on Marine Propulsors
smp'13, Launceston, Tasmania, Australia, May 2013

Converging Radial Velocity and Thrust Enhancement in Nature's Jetting Swimmers

Michael Krieg[1,3], **Kamran Mohseni**[1,2,3]

[1]Department of Mechanical and Aerospace Engineering,
[2]Department of Computer and Electrical Engineering,
[3]Institute for Networked Autonomous systems, University of Florida, Gainesville, Florida

ABSTRACT

A new underwater thruster design is inspired by propulsion mechanisms of jellyfish, squid, octopus and other cephalopods. The thruster expels finite jets of water periodically to provide necessary maneuvering forces on underwater vehicles and can be placed completely inside the vehicle body. Since the design is inspired by squid and jellyfish propulsion, this paper will investigate one way in which propulsive thrust is improved by these animals. A CFD simulation of a swimming jellyfish is analyzed to determine propulsive performance with respect to jetting kinematics, showing that the shape of the velar opening flaps induce a converging radial velocity in the jet increasing the total jet impulse. A prototype thruster was equipped with a set of nozzles to create both parallel and converging jet flows and it was observed that the converging jet flow produced a propulsive jet with $\approx 70\%$ more impulse than the parallel jet flow.

Keywords

Pulsed Jet, Biomimicry, Vortex Formation, Radial Velocity.

1 INTRODUCTION

The locomotion of squid and jellyfish inspired a novel type of thruster which generates propulsive forces by successively ingesting and expelling jets of water; and the thrust output of the device was characterized with respect to driving frequency and a jet parameter called the stroke ratio in Krieg & Mohseni (2008, 2010). One advantage of this thruster is that it can be placed within the hull of the vehicle with no protruding, drag-inducing parts as can be seen in Figure 1 which shows a vehicle testbed with these thrusters installed. This allows for a hybrid class vehicle with the efficient cruising characteristics of long range, torpedo shaped vehicles and the accurate maneuvering of bulky ROVs. The intricacies of squid and jellyfish swimming patterns should be studied in great detail to ensure that all propulsively-beneficial behaviors are accurately captured in mechanical representations.

As will be shown later in Figure 4 jellyfish induce a significant converging radial velocity. The squid funnel also changes shape during pulsation ranging from a straight tube to a converging cone resulting in a converging radial velocity. However, it is not immediately clear whether the converging radial velocity augments the jet propulsive force, because there are multiple competing objectives involved with biological jetting, including feeding and respiration (Lipinski & Mohseni (2009)). Additionally, laboratory experiments on starting jets are dominated by parallel jet flows, meaning that the flow is ejected through a long cylindrical tube creating parallel streamlines prior to ejection, which is clearly not a restriction for biological jetters. This paper identifies the effect that converging radial velocity has on the total impulse of starting jets as well as the pressure at the jetting source. This analysis is validated experimentally using a prototype jet thruster and is used to examine jellyfish jetting.

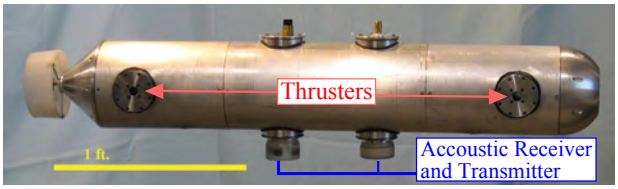

Figure 1: A prototype vehicle using the squid inspired thrusters of this investigation. The novel thruster provides the vehicle with accurate maneuvering capabilities without compromising the streamlined shape (Krieg et al. (2011)).

2 THRUSTER DESCRIPTION

The thruster consists of an internal fluid cavity which is exposed to the external flow via some form of nozzle. Two nozzle configurations which are discussed in this paper are shown in Figure 2. The first nozzle is essentially a thin flat plate with a central circular orifice, and is called an orifice nozzle. The second nozzle is a long cylindrical tube with a very sharp taper angle, γ, at the exit, and is termed a tube nozzle. Both nozzles have an opening of diameter D. The tube nozzle is sufficiently long ($> 6D$) to ensure that the jet flow is parallel before exiting the nozzle. Con-

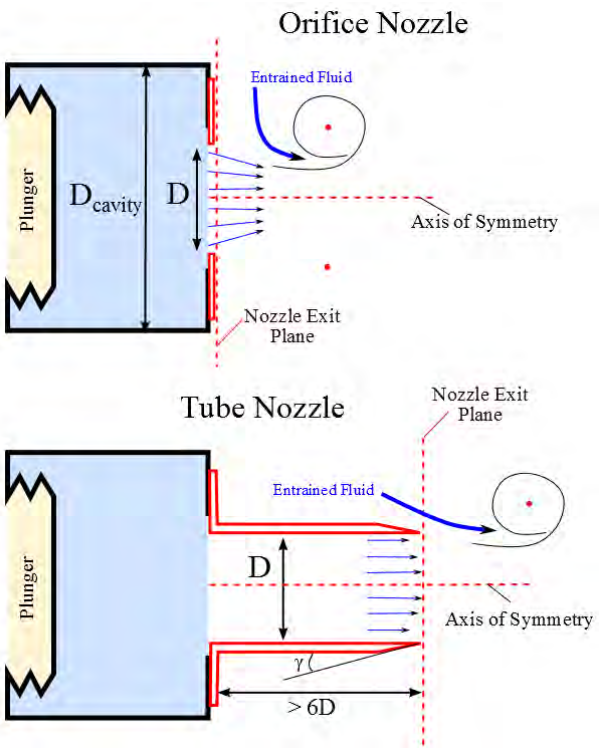

Figure 2: Schematic diagram of the thruster layout and different possible nozzle arrangements.

versely, the orifice nozzle creates a substantial converging radial velocity as much of the internal fluid must converge before passing through the orifice.

Within the internal cavity is a mechanism driving the fluid through the nozzle. The thruster of this investigation uses a semi-flexible plunger (illustrated in Figure 2) which can expand and contract in the axial direction but maintains a constant diameter like an accordion style bellows. However, there are a wide variety of options for this driving mechanism, including a sealed piston, piezo or rubber diaphragm, or flexible cavity.

After each jet pulsation, the cavity must be refilled through the same opening that the jet was expelled from. Jellyfish refill through the same opening, but squid actually have separate vents behind the head used for refilling the mantle cavity (Gosline & DeMont (1985)), as is depicted in Figure 3. Though squid use the separate vents they are still on the same side of the body as the funnel (jetting nozzle), suggesting that losses associated with this refilling mechanism might be minimized under certain conditions.

3 JET IMPULSE

The hydrodynamic impulse of a control volume, CV, is defined as,

$$\vec{I} \equiv \frac{1}{2}\int_{CV} \vec{x} \times \vec{\omega}\, d\vec{x}\,. \tag{1}$$

It was shown by Lamb (1945) (and in vector form by Saffman (1992)) that the rate of change of the hydrodynamic impulse is equal to the total non-conservative body

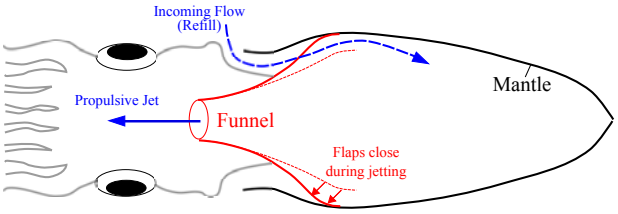

Figure 3: Diagram of squid anatomy showing separate inlet and outlet locations.

forces acting on the fluid. The total momentum of the control volume, $\vec{H} = \int \vec{u}\, d\vec{x}$, is not in general equal to the hydrodynamic impulse. Classical analysis by Cantwell (1986), has shown that the relationship is $H = \frac{2}{3} I_h$ for an unbounded spherical control volume. Therefore, the thrust generated by a propulsive jet should be calculated as the rate of change of the hydrodynamic impulse, not the fluid momentum. Krieg & Mohseni (2013) derived the rate of axial hydrodynamic impulse created in an axisymmetric jet flow with no swirl as,

$$\frac{dI}{dt} = \rho\pi \int_0^\infty 2u^2 r + u\frac{dv}{dx} r^2 - v^2 r\, dr\,, \tag{2}$$

where u and v are the axial and radial velocities along the plane where the propulsive jet is ejected (nozzle exit plane, see Figure 2) and ρ is the fluid density. This equation is valid provided that the fluid is incompressible and inviscid, generally corresponding to jet flows with Reynolds number $Re \geq 2000$ (see Mohseni et al. (2001)). The 1D slug model, which is generally used to approximate starting jet bulk quantities like impulse, assumes that the jet is expelled as a uniform slug of fluid resulting in,

$$\frac{dI}{dt} = \frac{\rho\pi}{2} u_p^2 R^2\,, \tag{3}$$

where R is the nozzle radius and u_p is the piston velocity (uniform slug velocity) which is defined, for any jet flow, as the volume flux divided by the nozzle area. Despite the widespread use of the slug model in approximating jet flows (Glezer (1988); Shariff & Leonard (1992); Gharib et al. (1998)), it is shown to be a poor predictor of jet impulse for both orifice nozzle jets (Krieg & Mohseni (2013)) and tube nozzle jets at or below the formation number (Krueger & Gharib (2005)). Therefore, later sections will calculate jellyfish and thruster impulse from both the exact entrance velocity profile (2) and the 1D slug model approximation (3).

4 JELLYFISH LOCOMOTION

Swimming jellyfish generate propulsion by ejecting the fluid in the velar/subumbrellar cavity through the velar opening flaps at a high velocity transferring significant momentum to the jellyfish. The most distinct jetting patterns and higher jetting velocities are seen in prolate jellyfish like *Sarsia tubulosa* (Ford & Costello (2000); Colin & Costello

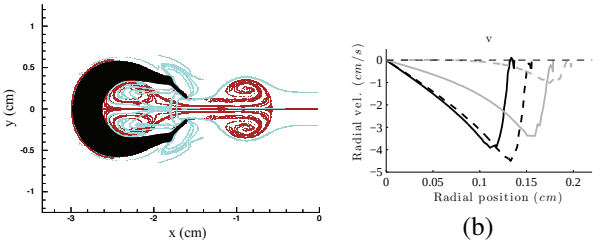

(a) (b)

Figure 4: A swimming jellyfish, *Sarsia tubulosa*, is shown along with stable (blue) and unstable (red) Lagrangian Coherent Structures (LCS)(a). Local radial velocity at the velar opening is plotted for several instances in (b). Data reproduced from Sahin et al. (2009); Lipinski & Mohseni (2009).

(2002)). The body shape (excluding tentacles) and vortex structures of a swimming *Sarsia tubulosa* are shown in Figure 4. The vortex structures are illustrated by Lagrangian coherent structures (LCS) as calculated from the velocity field by Lipinski & Mohseni (2009). The LCS are material transport barriers both forward and backward in time. Figure 4b shows the radial velocity profile in the jet at various times throughout the jetting cycle indicating a substantial converging radial velocity. Therefore, analysis of this propulsion mechanism based on parallel jet models will fail to address this important parameter.

4.1 Velar Morphology and Simulation

The exact body shape of a swimming *Sarsia tubulosa*, was filmed at high speed and the film analyzed to recover body outlines over several jetting cycles. The body shape at the start of locomotion is shown in Figure 5. The physical surfaces were then imported into a direct numerical simulation (DNS), which integrated fluid velocity from rest to produce the global velocity field at every time in the jetting process (Sahin & Mohseni (2009)). The velocity and pressure fields calculated from this process were used to evaluate and compare the propulsive performances of *Sarsia tubulosa* and *Aequorea Victoria* (Sahin et al. (2009)), and were analyzed with respect to material transport barriers by Lipinski & Mohseni (2009) showing how the vortex ring produced by the jet aids in feeding of both species.

The present study examines in particular how the velar flap morphology affects the jet kinematics at the nozzle exit plane (see Figure 5), and the resulting propulsive forces. The first jetting cycle is analyzed, meaning that both the jellyfish and surrounding fluid start at rest. The piston velocity and velar opening radius are plotted for the first jetting cycle in Figure 6. In general the jellyfish contracts the bell together to expel the propulsive jet, and as this takes place, the velar flaps (see Figure 5) are brought together, but also swing outward in the direction of the jet deforming the 'nozzle' from a flat plate to a converging cone. As can be seen in Figure 6b the opening radius contracts, along

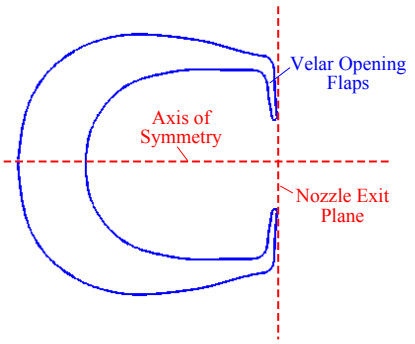

Figure 5: Body shape of a swimming *Sarsia tubulosa* reconstructed from high speed filming.

with the jetting area, despite the outward flexing velar flaps. Figure 6a shows that the piston velocity accelerates for the majority of pulsation, trailing off at the end as the jellyfish body relaxes. Much of the piston velocity acceleration can be attributed to the reduction in jetting area (nozzle radius) with very little acceleration in total volume flux during jetting, which reduces the overall load on the jellyfish required to create larger piston velocities at later stages of jetting.

4.2 Thrust Enhancement

The total hydrodynamic impulse of the jellyfish propulsive jet is calculated from the DNS velocity field of the wake assuming symmetry about the central axis,

$$I = \pi \int_{x_n}^{\infty} \int_{0}^{\infty} \omega r^2 dr dx \tag{4}$$

where x_n is the axial location of the nozzle exit plane (see Figure 5) and ∞ refers to the edge of the computational domain in both axial and radial directions. It should be noted that as the jellyfish is swimming and deforming the nozzle exit plane moves through the domain. Equation (2) was derived by calculating the derivative of equation (1) assuming a stationary control volume. Additional terms must be included for a control volume with moving boundaries amending equation (2) to,

$$\frac{dI}{dt} = \rho\pi \int_{0}^{\infty} 2u\,(u-u_b)\,r + (u-u_b)\,\frac{dv}{dx}r^2 - v^2 r\,dr\,, \tag{5}$$

where u_b is the velocity of the nozzle exit plane in the inertial frame. The total impulse measured in the propulsive jet over the first jetting cycle is plotted in Figure 7. The total impulse transfered to the jet is also approximated by the 1D slug model (3) from the piston velocity and nozzle radius profiles, Figure 6, and calculated from the exact velocity profiles at the nozzle exit plane (5). Both of these calculations are defined in terms of impulse transfer rates, which are integrated to predict total jet impulse and plotted in Figure 7.

It can be seen in Figure 7 that the total jet impulse is noticably higher than the 1D slug model prediction. The 1D

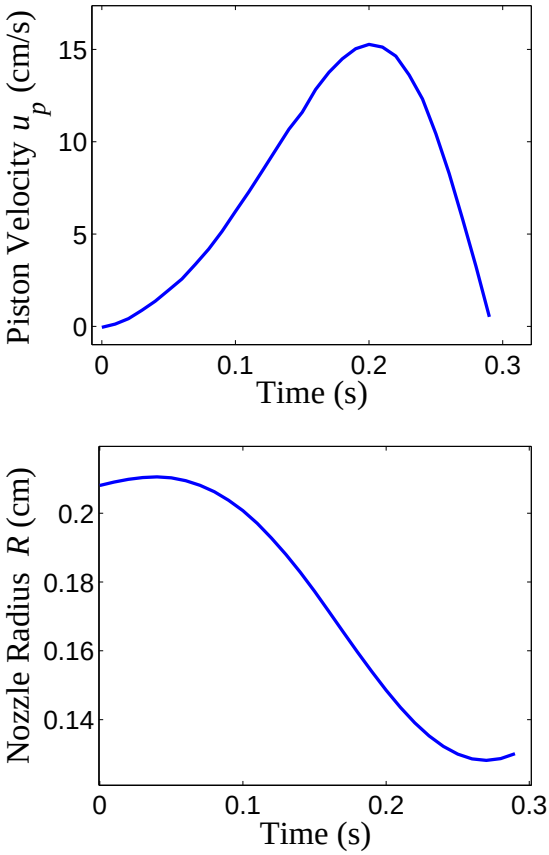

Figure 6: Piston velocity, u_p, (a) and velar opening radius (b) of a swimming *Sarsia tubulosa* jellyfish during the 1'st jetting cycle.

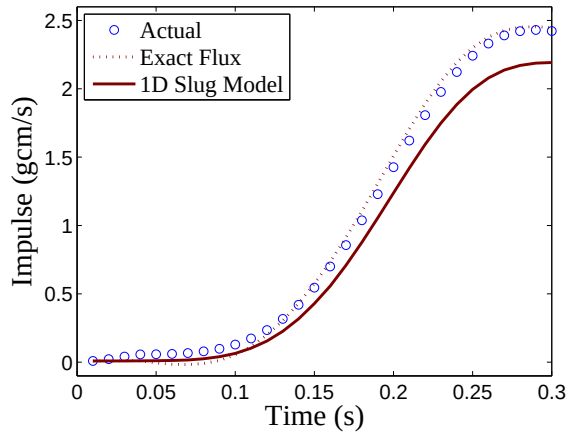

Figure 7: Total impulse of the jellyfish propulsive jet as a function of time.

slug model can be considered equivalent to the impulse created by a parallel jet with identical piston velocity and nozzle radius (identical volume flux); therefore, the converging radial velocity improves the propulsive performance of the jet. The total jet impulse predicted by the exact flux across the nozzle exit plane predicts an impulse which is larger than the impulse of the jet calculated from the DNS velocity field. This is due to the fact that the jellyfish is swimming with a relatively low Reynolds number ($Re = 1195$ calculated from the jet circulation, $Re = \Gamma/\nu$), where viscous dissipation becomes a factor, though viscous effects are still fairly minimal. Since the propulsive force is related to the total impulse transfer, and is unaffected by the dissipation as the jet evolves downstream. The impulse transfer rate determined from (2) should be considered the propulsive force rather than the derivative of the total impulse determined from DNS. Therefore, Figure 7 shows that the converging radial velocity increases the total impulse transfer by more than 12% over the impulse of a parallel jet with identical volume flux.

Following the example of the jellyfish we test a prototype thruster equipped with both tube and orifice nozzles. For both cases the nozzle diameter, total jet volume, piston velocity, and jet stroke ratio are identical measuring, $D = 0.91$cm, $Vol = 33$ ml, $u_p = 7$cm/s, and $L/D = 7$, respectively. The jet produced from the prototype thruster is illuminated by a laser sheet in cross section (bisecting the axis of symmetry), seeded with reflected particles and filmed with a high speed camera. Standard DPIV techniques similar to algorithms described in Willert & Gharib (1991) and Raffel et al. (1998) were used to calculate the jet velocity field including the velocity profiles at the nozzle exit plane. The total jet impulse as calculated from (4) is shown for the two cases as well as the impulse calculated from the 1D slug model (3) and exact flux terms (2) in Figures 8a and 8b. For this case the thruster is rigidly fixed in place ($u_b = 0$) and equation (5) collapses back into (2).

The jet flow of the prototype thruster has a significantly higher Reynolds number than the jellyfish jet, meaning that viscosity does not have a significant effect on the total jet impulse. As a result the total jet impulse measured from DPIV is very close to the total impulse calculated by integrating the rate of impulse from the exact flux equation (2), for both parallel and converging jet flows. The parallel jet flow (tube nozzle Figure 8a) actually results in an impulse lower than is predicted by the 1D slug model for parallel flows. This is due to the interaction of the jet flow with entrained fluid at the nozzle exit plane which is discussed in greater detail in Krieg & Mohseni (2013), but the exact flux terms still calculate the total impulse accurately. The orifice nozzle expels a jet with a maximum amount of converging radial velocity for the entire duration of pulsation, and the enhancement of total jet impulse is substantial. Taking into account the fact that the parallel jet (tube nozzle) is slightly

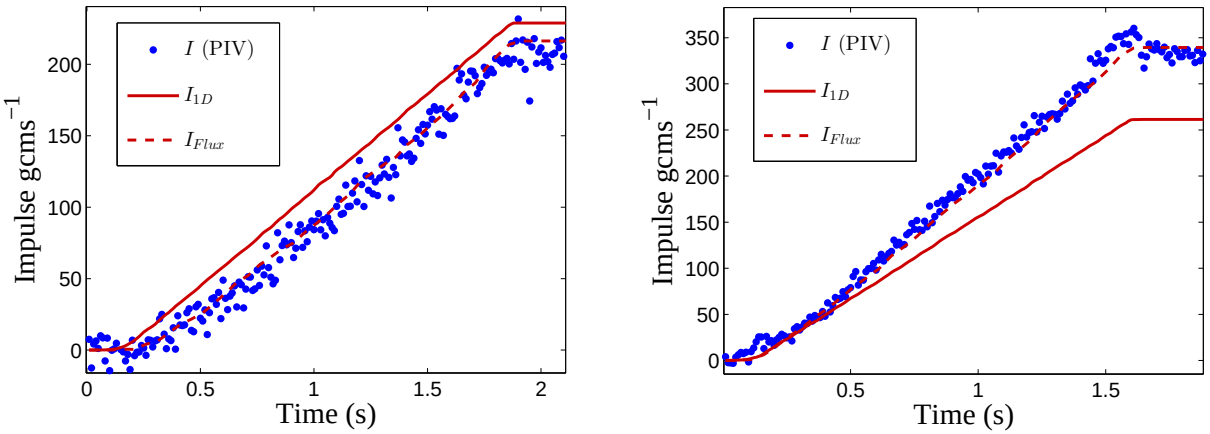

Figure 8: Total jet impulse is shown as a function of pulsation time for both parallel (a) and converging (b) starting jets. For both jet flows the piston velocity is $u_p = 7$cm/s and the jet stroke ratio is $L/D = 7$. I_{1D} represent the values calculated from the 1D slug model (3), I_{Flux} are the values calculated from the exact velocity profiles (2), and I(PIV) are the values measured directly from PIV data (4).

below the 1D slug model prediction, the orifice nozzle produces a propulsive jet with $\approx 70\%$ more impulse than the tube nozzle for identical volume flow rates and nozzle diameters.

CONCLUSIONS

It is important not to overlook the lessons learned by marine animals through millions of years of evolution. However, it is just as important to qualify those lessons and determine where improvements can be made in mechanical systems which do not have the same limitations as those animals. Squid and jellyfish demonstrate that successively ingesting and expelling finite jets of water is a viable propulsion option for small scale vehicles, and that the thrust from this jetting can be enhanced by inducing a converging radial velocity in the propulsive jet. However, it is important to recognize that behavior and morphology of organisms like jellyfish are often motivated by multiple goals, such as feeding and respiration in addition to locomotion, and exact replication may not be the optimal solution. A prototype thruster was outfitted with a nozzle inducing the maximum amount of converging radial velocity for the entire pulsation, and the impulse of the jet was observed to increase by as much as 70% over a parallel with identical volume flux which is much greater than the 20% improvement seen for the jellyfish jetting.

REFERENCES

Cantwell, B., 1986. 'Viscous Starting Jets'. J. Fluid Mech., **173**, pp. 159–189.

Colin, S. & Costello, J., 2002. 'Morphology, swimming performance and propulsive mode of six co-occuring hydromedusae'. J. Exp. Biol., **205**, pp. 427–437.

Ford, M. & Costello, J., 2000. 'Kinematic comparison of bell contraction by four species of hyromedusae'. Sci. Mar., **64**, pp. 47–53.

Gharib, M., Rambod, E. & Shariff, K., 1998. 'A universal time scale for vortex ring formation'. J. Fluid Mech., **360**, pp. 121–140.

Glezer, A., 1988. 'The formation of vortex rings'. Phys. Fluids, **31**(12), pp. 3532–3542.

Gosline, J. & DeMont, E., 1985. 'Jet-propelled swimming in squids'. Sci Am, **252**, pp. 96–103.

Krieg, M., Klein, P., Hodgkinson, R. & Mohseni, K., 2011. 'A Hybrid class underwater vehicle: bioinspired propulsion, embedded system, and acoustic communication and localization system'. Marine Technology Society Journal: Special Edition on Biomimetics and Marine Technology, **45**(4), pp. 153 – 164.

Krieg, M. & Mohseni, K., 2008. 'Thrust Characterization of Pulsatile Vortex Ring Generators for Locomotion of Underwater Robots'. IEEE J. Oceanic Engineering, **33**(2), pp. 123–132.

Krieg, M. & Mohseni, K., 2010. 'Dynamic modeling and control of biologically inspired vortex ring thrusters for underwater robot locomotion'. IEEE Trans. Robotics, **26**(3), pp. 542–554.

Krieg, M. & Mohseni, K., 2013. 'Modelling circulation, impulse, and kinetic energy of starting jets with non-zero radial velocity'. J. Fluid Mech., **Accepted**.

Krueger, P. & Gharib, M., 2005. 'Thrust augmentation and vortex ring evolution in a fully pulsed jet'. AIAA J., **43**(4), pp. 792–801.

Lamb, H., 1945. Hydrodynamics. Dover, New York.

Lipinski, D. & Mohseni, K., 2009. 'Flow structures and fluid transport for the hydromedusae *Sarsia tubulosa* and *Aequorea victoria*'. J. Exp. Biol., **212**, pp. 2436–2447.

Mohseni, K., Ran, H. & Colonius, T., 2001. 'Numerical experiments on vortex ring formation'. J. Fluid Mech., **430**, pp. 267–282.

Raffel, M., Willert, C. E. & Kompenhans, J., 1998. Particle Image Velocimetry. Springer, Heidelberg, NY.

Saffman, P., 1992. Vortex Dynamics. Cambridge University Press, Cambridge.

Sahin, M. & Mohseni, K., 2009. 'An arbitrary Lagrangian-Eulerian formulation for the numerical simulation of flow patterns generated by the hydromedusa *Aequorea victoria*'. J. Comp. Physics, **228**, pp. 4588–4605.

Sahin, M., Mohseni, K. & Colins, S., 2009. 'The numerical comparison of flow patterns and propulsive performances for the hydromedusae *Sarsia tubulosa* and *Aequorea victoria*'. J. Exp. Biol., **212**, pp. 2656–2667.

Shariff, K. & Leonard, A., 1992. 'Vortex rings'. Ann. Rev. Fluid Mech., **34**, pp. 235–279.

Willert, C. & Gharib, M., 1991. 'Digital particle image velocimetry'. Experiments in Fluids, **10**, pp. 181–193.